particular, the formation of novel flowerlike structures. The observation of coexisting multiple morphologies in diblock copolymer systems of narrow polydispersity has been previously reported,[15] whereas (as mentioned above) recent work has provided examples of systems in which well-defined aggregates are formed despite significant polydispersities (PDI = 1.6).[12] In our particular case, fractionation experiments suggest that the composition variations associated with the polydispersity of the sample (PDI = 1.4) play a critical role in determining the morphologies observed. Future work will focus on gaining further detailed understanding of the factors that influence the formation of the observed supramolecular organometallic polymer structures. In addition, PFS is redox-active: Upon oxidation it becomes a semiconductor, and on pyrolysis it forms magnetic ceramics. Therefore, the possibility of accessing nanoscale assemblies with intriguing physical properties is also of considerable interest.[9,10]

Experimental Section

Samples for TEM were prepared by aerosol spraying a dilute micellar solution (ca. 50 μL, ca. 10^{-4} mg mL^{-1}) onto a thin carbon film (ca. 10 Å) grown on mica and then floated off the mica and placed on 200-mesh gilder copper TEM grids. Transmission electron micrographs were obtained on a Hitachi model 600 electron microscope. Samples for AFM were prepared by aerosol spraying a dilute micellar solution (ca. 50 μL, ca. 10^{-4} mg mL^{-1}) onto freshly cleaved mica. The AFM images were obtained using a Nanoscope III microscope (Digital Instruments) in the tapping mode with a silicon cantilever with a resonance frequency of 300–380 kHz. The GPC data were obtained in THF and are relative to polystyrene standards, and the values are therefore considered to be estimates.

3a: To a solution of **2** (1.16 g, 4.79 mmol) and SiH-terminated PDMS (1.44 g, 0.24 mmol, $M_w = 6.02 \times 10^3$, PDI = 1.24) in toluene (20 mL) was added an aliquot (43 μL) of a 0.3% (by weight) solution of Karstedt's catalyst in xylenes. After stirring for 24 h, the deep orange solution was precipitated into methanol (150 mL). The orange precipitate was washed with methanol (3 × 100 mL) and dried under vacuum. Yield: 1.95 g (75%). GPC: $M_n = 8.14 \times 10^3$, PDI = 1.45; ^{1}H NMR (400 MHz, C_6D_6): $\delta = 0.28$ (s, 21 H, OSi$(CH_3)_2$O), 0.54 (s, 6 H, fcSi$(CH_3)_2$fc), 4.09 (m, 4 H, α- or β-C_5H_4), 4.26 (m, 4 H, α- or β-C_5H_4); ^{29}Si{^{1}H} NMR (79.5 MHz, C_6D_6, DEPT J = 51 Hz): $\delta = -21.4$ (s, OSi$(CH_3)_2$O), -18.2 (s, fcSi$(CH_3)_2$H), -6.38 (s, fcSi$(CH_3)_2$fc), 0.7 (s, fcSi$(CH_3)_2$O); fc = $(C_5H_4)_2$Fe.

3b: To a solution of **2** (1.73 g, 7.14 mmol) and SiH-terminated PDMS (5.0 g, 0.25 mmol, $M_w = 2.00 \times 10^4$, PDI = 1.60 (GPC)) in toluene (40 mL) was added an aliquot (64 μL) of a 0.3% (by weight) solution of Karstedt's catalyst in xylenes. After stirring for 24 h, the deep orange solution was precipitated into methanol (250 mL). The adhesive orange gum was washed with methanol (3 × 200 mL) and dried under vacuum. Yield: 4.8 g (71%). GPC: $M_n = 2.88 \times 10^4$, PDI = 1.43; ^{1}H NMR (400 MHz, C_6D_6): δ = 0.28 (s, 39 H, OSi$(CH_3)_2$O), 0.55 (s, 6 H, fcSi$(CH_3)_2$fc), 4.10 (m, 4 H, α- or β-C_5H_4), 4.27 (m, 4 H, α- or β-C_5H_4); ^{29}Si{^{1}H} NMR (79.5 MHz, C_6D_6, DEPT J = 51 Hz): $\delta = -21.4$ (s, OSi$(CH_3)_2$O), -6.4 (s, fcSi$(CH_3)_2$fc).

Received: March 15, 1999 [Z13163IE]
German version: *Angew. Chem.* **1999**, *111*, 2738–2742

Keywords: copolymerizations · nanostructures · polymers · self-assembly · supramolecular chemistry

[1] S. Förster, M. Antonietti, *Adv. Mater.* **1998**, *10*, 495.
[2] F. S. Bates, *Science* **1991**, *251*, 898.
[3] J. P. Spatz, S. Mössmer, M. Möller, *Angew. Chem.* **1996**, *108*, 1673; *Angew. Chem. Int. Ed. Engl.* **1996**, *35*, 1510.
[4] For recent work on nonspherical micellar aggregates of organic block copolymers in solution, see for example C. Price, *Pure Appl. Chem.* **1983**, *55*, 1563; M. Antonietti, S. Heinz, M. Schmidt, C. Rosenauer, *Macromolecules* **1994**, *27*, 3276; L. Zhang, A. Eisenberg, *Science* **1995**, *268*, 1728; L. Zhang, K. Yu, A. Eisenberg, *Science* **1996**, *272*, 1777; Y. Yu, A. Eisenberg, *J. Am. Chem. Soc.* **1997**, *119*, 8383; J. Tao, S. Stewart, G. Liu, M. Yang, *Macromolecules* **1997**, *30*, 2738.
[5] For recent intriguing examples of nanostructured materials based on block copolymers, see S. Förster, M. Antonietti, *Adv. Mater.* **1998**, *10*, 195; C. C. Cummins, R. R. Schrock, R. E. Cohen, *Chem. Mater.* **1992**, *4*, 27; G. Liu, J. Ding, *Adv. Mater.* **1998**, *10*, 69; G. Liu, *Adv. Mater.* **1997**, *9*, 437; K. L. Wooley, *Chem. Eur. J.* **1997**, *3*, 1397; M. Moffitt, H. Vali, A. Eisenberg, *Chem. Mater.* **1998**, *10*, 1021; J. Spatz, S. Mössmer, M. Möller, M. Kocher, D. Neher, G. Wegner, *Adv. Mater.* **1998**, *10*, 473.
[6] R. Rulkens, Y. Ni, I. Manners, *J. Am. Chem. Soc.* **1994**, *116*, 12121.
[7] Y. Ni, R. Rulkens, I. Manners, *J. Am. Chem. Soc.* **1996**, *118*, 4102.
[8] J. Massey, K. N. Power, I. Manners, M. A. Winnik, *J. Am. Chem. Soc.* **1998**, *120*, 9533.
[9] a) I. Manners, *Can. J. Chem.* **1998**, *76*, 371; b) J. Massey, K. N. Power, M. A. Winnik, I. Manners, *Adv. Mater.* **1998**, *12*, 1559; c) I. Manners, *Chem. Commun.* **1999**, 857.
[10] In addition, the formation of magnetic nanostructures upon pyrolysis of cylinders of PFS in mesoporous silica, MCM-41, has been demonstrated; see for example M. J. MacLachlan, P. Aroca, N. Coombs, I. Manners, G. A. Ozin, *Adv. Mater.* **1998**, *10*, 144.
[11] P. Gómez-Elipe, R. Resendes, P. M. Macdonald, I. Manners, *J. Am. Chem. Soc.* **1998**, *120*, 8348.
[12] S. J. Holder, R. C. Hiorns, N. A. J. M. Sommerdijk, S. J. Williams, R. G. Jones, R. J. M. Nolte, *Chem. Commun.* **1998**, 1445.
[13] Similar morphologies have been observed in the precipitation of calcium phosphate in the presence of double-hydrophilic block copolymers: M. Antonietti, M. Breulmann, C. G. Göltner, H. Cölfen, K. K. W. Wong, D. Walsh, S. Mann, *Chem. Eur. J.* **1998**, *4*, 2493.
[14] To investigate the reproduciblity of micelle formation as well as the possible separation of the different micellar morphologies, an additional micellar solution was prepared employing the same dialysis methodology mentioned above. When this solution of **3b** in *n*-hexane was examined by TEM after solvent evaporation the same micellar assemblies were observed.
[15] K. Yu, A. Eisenberg, *Macromolecules* **1996**, *29*, 6359.

Identification of Triplet States in Carotenoids by Intracavity Absorption Spectroscopy and Measurements of Delayed Fluorescence**

Hans Bettermann,* Lars Ulrich, Gabriele Domnick, and Hans-Dieter Martin

Carotenoids have two important functions in nature: the absorption of solar energy and the subsequent radiationless energy transfer to chlorophyll or bacteriochlorophyll at the beginning of photosynthesis as well as the quenching of triplet states of chlorophyll, which generate singlet oxygen, and the quenching of already generated singlet oxygen. While it has

[*] Priv.-Doz. Dr. H. Bettermann, Dipl.-Chem. L. Ulrich
Institut für Physikalische Chemie und Elektrochemie der Universität
Universitätsstrasse 1, D-40225 Düsseldorf (Germany)
Fax: (+49) 211-8115195
E-mail: betterma@uni-duesseldorf.de

Dipl.-Chem. G. Domnick, Prof. Dr. H.-D. Martin
Institut für Organische Chemie und Makromolekulare Chemie der Universität Düsseldorf (Germany)

[**] We are grateful to the Fonds der Chemischen Industrie for financial support.

been discussed to what extent energy transfer is initiated by singlet states of carotenoids,[1] it is commonly accepted that the lower energetic triplet states protect the carotenoids from oxidation.[2] Despite their biological importance very little experimental data is available on the energy of the triplet states in carotenoids. The main reason for this is the extraordinarily low quantum yield of phosphorescence which excludes direct measurements. Consequently, only one article has appeared in which phosphorescence measurements on β-carotene are reported.[3] The energies of triplet states are therefore mainly obtained indirectly by quenching experiments,[4] by extrapolation[5] based on the correlation between chain lengths and triplet energies, and by photoacoustic calorimetry.[6] Estimations by extrapolation originate from measurements of triplet energies of short-chain polyenes by electron-impact-spectroscopy in gas phase.[7]

Herein we report on intracavity absorption measurements[8] and measurements of delayed fluorescence which enabled us to determine the energies of triplet states in carotenoids directly.

For the intracavity spectroscopy the sample is part of the dye laser resonator. By inserting a light absorbing sample within the resonator the number of the laser photons is reduced, causing a strong decrease of the outcoupled laser intensity. The magnitude of the latter quantity determines the absorbance of the sample. By tuning the wavelengths of the dye laser, the laser power as a function of the wavelength yields the intracavity absorption spectrum.

The measurements were carried out on the compound 8,13-dimethyl-2,2,19,19-tetramethoxyicosa-4,6,8,10,12,14,16-heptaene-3,18-dione (**1**). Like the natural carotenoids this compound has an isoprenoid structure but in comparison to them it is highly photostable. As the natural all-*trans* carotenoids, **1** is C_{2h}-symmetric, which can be derived by analyzing the IR and Raman spectra.

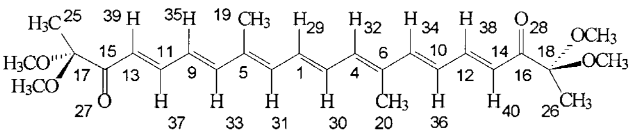

1

Before recording optically forbidden transitions it is useful to determine the number of electronic states in question and to estimate their energetic sequence. This was carried out by applying AM1 calculations that include configurational interactions (C.I. = 4, 70 different microstates). By analogy with long-chain all-*trans* polyenes,[9] the first two excited states are triplet states; the energy gap of about 1300 cm^{-1} between the T_2 state and the first excited singlet state is very small.

The states $S_0(A_g) < T_1(11277\ cm^{-1}, B_u) < T_2(20515\ cm^{-1}, A_g) < S_1(21806\ cm^{-1}, A_g) < S_2(23651\ cm^{-1}, B_u) < T_3(30582\ cm^{-1}, B_u)$ generated by singly excited microstates are electronic levels which belong to odd symmetry species, whereas the remaining excited states consist of doubly excited microstates. Electronic excitations between states of different parity are optically allowed and are characterized by large absorptivities. Thus, the $S_0 \rightarrow S_2$ transition dominates the UV/Vis absorption spectrum. The first band maximum lies at 20660 cm^{-1} (S_0-S_2: $\varepsilon_{484\,nm} = 104000\ L\,mol^{-1}\,cm^{-1}$ in $CHCl_3$).

Since transitions between states of the same parity are optically forbidden, it can be expected that the absorptivities of the S_0-S_1 transition and S_0-T_2 transition are very small. The symmetry selection rules can be partially weakened by Herzberg–Teller coupling[10] so that these transitions can be made visible by sensitive spectroscopic methods. In the case of vibronic Herzberg–Teller coupling, for **1** an electronically excited state of symmetry A_g couples with an electronic state of species B_u via a non-totally symmetric mode of b_u-type.

For the identification of the non-totally symmetric b_u-promoting modes, a vibrational analysis was carried out based on the aforementioned AM1 approach. The calculations reveal that the vibrations of the electronically excited states differ only slightly in their frequencies and the vibrational form from those of the electronic ground state. Thus the ground state vibrations were used for the assignment of the vibronic transitions. The eigenvectors of the calculated vibrations were used to obtain the symmetry species of the vibrational modes. Between 50 and 1700 cm^{-1} all b_u fundamental modes could be identified in the IR spectrum, while all a_g vibrations were found in the Raman spectrum. These vibrations could be assigned directly to the calculated frequencies without having to apply any scaling.

The energy of the S_1 state could be roughly estimated to be between 15000 and 16000 cm^{-1} by fluorescence spectra and fluorescence excitation spectra,[11] which are shaped by the promoting modes.

Figure 1 shows the intracavity absorption spectrum of **1** between 15400 and 16200 cm^{-1}.[12] Two different types of transitions are visible in the spectrum. Four broad bands at 15356, 15552, 15773, and 16077 cm^{-1} are accompanied by a sequence of weaker transitions. Three of these transitions (15552, 15773, and 16077 cm^{-1}) are also detectable in the fluorescence excitation spectrum as origins of luminescence. Because of this fluorescence behavior and the fact that the observed transitions generate subspectra within the absorp-

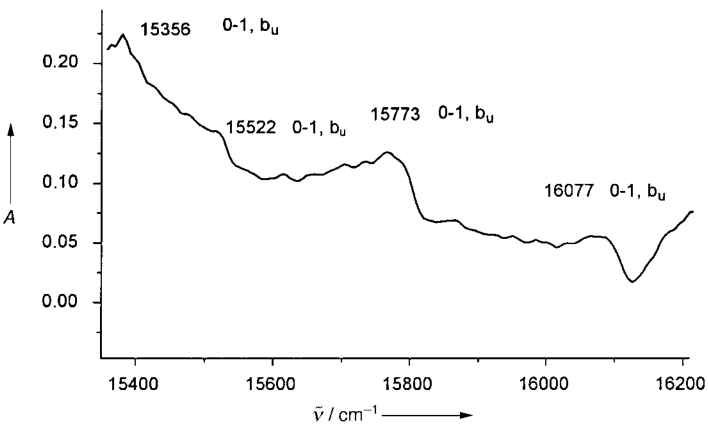

Figure 1. Intracavity absorption spectrum of **1** in the range of 15400–16200 cm^{-1}. Assignment of the bands to b_u modes of the S_1 state (notation: internal coordinate ([%] PED, portion of stretching motion)): 15356 cm^{-1}: b_u 152 cm^{-1}; C47–H57 (15.2, 0.9), C47–H61 (12.4, 11.1) 15522 cm^{-1}: b_u 318 cm^{-1}; C18–C26 (6.8, 0.0), C17–C25 (6.7, 0.0) 15773 cm^{-1}: b_u 569 cm^{-1}; C18–O24 (5.6, 0.8), C17–O23 (5.6, 0.8) 16077 cm^{-1}: b_u 873 cm^{-1}; C4–H32 (17.0, 0.0), C3–H31 (17.0, 0.0).

tion spectrum, these vibronic transitions are assigned to promoting modes.

Since the electronic origin of the symmetry-forbidden transition remains invisible, the 0–0 transition (15204 cm^{-1}) was identified by the sequence of the appearing promoting modes within the spectrum. While the $S_0 \rightarrow S_1$ spectrum was recorded at a concentration of 5×10^{-6} M (in ethanol), the transitions between 14800 and 15500 cm^{-1} could only be detected, if the concentration was increased to 4×10^{-4} M. (Figure 2) Owing to the resulting small absorptivities of these

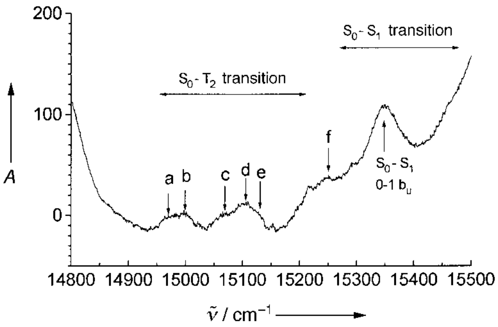

Figure 2. Intracavity absorption spectrum of **1** in the range of 14800–15500 cm^{-1}, a–f: vibronic S_0–T_2 transitions, see also Table 1.

transitions and in accordance with the calculated electronic energy of the T_2 state, these absorptions were assigned to vibronic S_0–T_2 transitions. The triplet character of the excited state was supported by luminescence measurements. If crystalline **1** is excited by dye laser light in the region from 13700 to 15200 cm^{-1}, three vibronically induced S_1–S_0 fluorescence bands between 15500 and 17000 cm^{-1} are observed (Figure 3). The marked tails of these broad electronic absorption bands coincide with Herzberg–Teller coupling induced vibronic transitions from the S_0–S_1 absorption spectrum.

By analogy with the fluorescence behavior of polycondensed hydrocarbons the observed emission of **1** is explained by the recombination of mobile triplet excitons and subsequent emission of S_1–S_0 fluorescence denoted as P-type delayed fluorescence.[13] Because of the low S_1–S_0 and S_2–S_0 fluorescence quantum yields as well as the high photochemical stability of **1**, the largest part of the excitation is transferred to the T_1 state by intersystem crossing (Ermolaev rule[14]). Therefore a sufficiently high occupation of the T_1 state can be expected for the recombination. The alternative

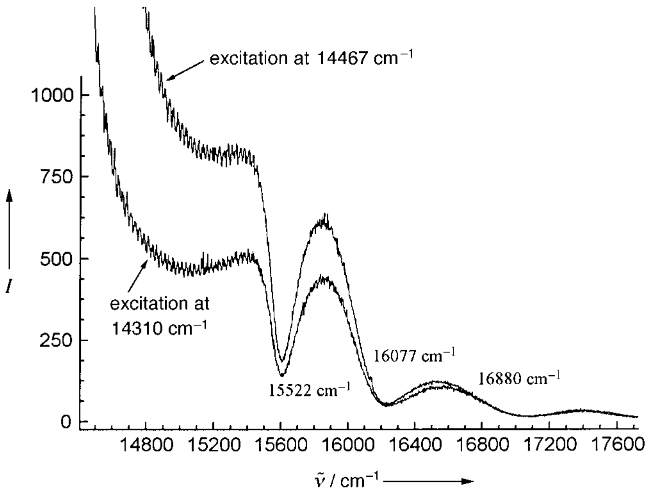

Figure 3. Spectrum of the delayed fluorescence, excitation (laser power 3 mW) at 14310 cm^{-1} and 14467 cm^{-1}. The rise of intensity at 14300 cm^{-1} is caused by Rayleigh scattering; the numbers indicate the tails of vibronically induced fluorescence bands. Assignment of the bands to b_u modes of the S_1 state: (notation: internal coordinate ([%] PED, portion of stretching motion)) 15522 cm^{-1}: b_u 318 cm^{-1}; C18–C26 (6.8, 0.0), C17–C25 (6.7, 0.0) 16077 cm^{-1}: b_u 873 cm^{-1}; C4–H32 (17.0, 0.0), C3–H31 (17.0, 0.0) 16880 cm^{-1}: b_u 1676 cm^{-1}; C15–O27 (29.1, 100), C16–O28(25.6, 100).

E-type of delayed fluorescence can be neglected since the large energy gap (3927 cm^{-1}) between the calculated T_1 state energy and the experimentally determined S_1 state energy (derived from the S_0–S_1 0–0 transition) excludes the thermal population of the first excited singlet state.

Since the T_2 state also has A_g symmetry, the S_0–T_2 transition has to be vibronically induced by Herzberg–Teller coupling in order to become visible. The transition wavenumbers of the bands a–f, which are detected in the intracavity absorption spectrum, were determined by a band-shape analysis. According to their mutual wavenumber differences, these transitions correspond to a certain sequence of transitions detected in the IR spectrum (Table 1). Alternative frequency ranges of the non-totally symmetric vibrations to that presented in Table 1 can be excluded because of the groups of transitions that appear in the IR spectrum and because of the frequency differences of adjacent IR transitions. Except for the transition at 15000 cm^{-1}, the detected vibronic transitions can be assigned to transitions that originate from fundamental modes. The band at 15000 cm^{-1} can be suitably assigned by choosing a pair of vibrations (569 and 200 cm^{-1}), since the non-totally symmetric mode at

Table 1. Non-totally symmetric modes for the Herzberg–Teller coupling of the S_0–T_2 spectrum (Figure 2). The 0–0 transition of the S_0–T_2 transition is calculated to be at 14233 cm^{-1}.

No.	Intracavity [cm^{-1}]	T_2 modes [cm^{-1}]	IR transitions [cm^{-1}]	Assignment (internal coordinate ([%] PED, portion of stretching motion))
a	14974	741	733	C18–O22 (5.8, 7.6), C16–O28 (5.7, 3.5)
b	15000	767	569	C18–O24 (5.6, 0.8), C17–O23 (5.6, 0.8)
			+200	C26–H54 (6.0, 5.3), C25–H53 (5.5, 5.4)
c	15067	834	826	C9–H35 (21.1, 0.0), C10–H36 (20.4, 0.0)
			836	C2–H30 (15.0, 0.0), C1–H29 (15.0, 0.0)
d	15105	872	872	C4–H32 (17.0, 0.0), C3–H31 (17.0, 0.0)
e	15130	897	890	C13–H39 (24.3, 0.0), C14–H40 (20.8, 0.0)
f	15243	1010	1010	C26–H52 (23.5, 20.8), C26–H54 (12.9, 3.6)

569 cm^{-1} was also identified as the promoting mode in the $S_0 \rightarrow S_1$ absorption spectrum. The mode at 200 cm^{-1} could be unambiguously assigned to a totally symmetric mode from the Raman spectrum. Two of the assigned vibrations (872, 890 cm^{-1}) were also detected in the S_0-S_1 absorption spectrum. From the complete sequence of non-symmetric vibrations shown in Table 1, the 0–0 transition of the S_0-T_2 transition can be calculated to be at 14233 cm^{-1}. This result coincides well with the calculated energy differences between the S_1 state and the T_2 state. The largest values of the PED (potential energy distribution) matrix elements show that the inducing modes contain bending-vibrational character to a large extent. The largest elongations take place at the terminal groups and along the polyene chain. The latter motions are induced by C–H bending modes. Considering the weak s-shape of the polyene chain in carotenoids,[15] the mentioned modes generate large geometrical distortions which are predistined for the Herzberg–Teller coupling.

In conclusion, the presented absorption and emission processes can be illustrated in a term diagram (Figure 4). The goal of this work was to show that energies of triplet states in carotenoids, which are important for the energy transfer and for the oxidative protection at the beginning of photosynthesis, can be determined by intracavity absorption spectroscopy and measurements of delayed fluorescence. In future work these methods will be applied to characterize the T_1 states of natural carotenoids.

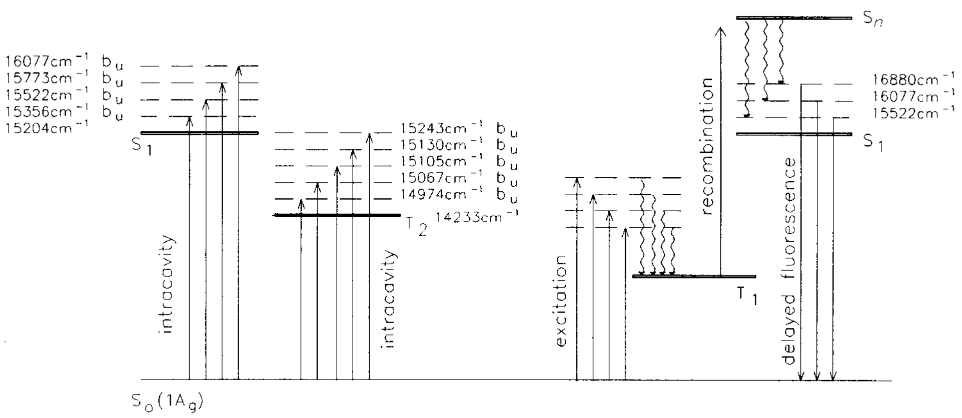

Figure 4. Term diagram for the delayed fluorescence with experimental energy data of **1**.

Experimental Section

The intracavity absorption spectra were carried out within a dye laser (Spectra Physics, model 375, Rhodamin 101 14800-151 750 cm^{-1}, Pyridin1 13800–14700 cm^{-1}) whose resonator was extended by about 50 cm. To avoid interferences, the sample cell (Hellma 111-QS, 1 cm) was slightly tilted with respect to the resonator axis. An aperture was inserted directly in front of the outcoupling mirror. The sample cell was rigidly clamped into the sample holder in order to exclude alterations of the sample position by the refill process. The excitation wavelengths were obtained by positioning a tuning wedge (free spectral range: 100 THz) which was inserted inside the resonator. The tuning of the wedge was carried out in steps of 0.6 cm^{-1} by a stepper motor. A monochromator (Jobin Yvon, model THR1500, focal length: 1.5 m) was used to check the selected dye laser wavelength. The outcoupled laser power was detected by a photodiode (BPW20), which was uniformly illuminated. Its analogous signals were digitalized by a 16-Bit A/D converter. The absorption signals, obtained by subtracting the laser signals of the solution from that of the solvent, amount 50–100 counts, while the noise has 4 counts. The fluorescence and the Raman signals of crystalline **1** were obtained by exciting the sample with focused light of the above-mentioned dye laser. The emitted light was dispersed by a Czerny–Turner-type double monochromator (Jarrell Ash, model 25-400, focal length: 1 m, spectral resolution was set to 20 cm^{-1} at 16000 cm^{-1}) and detected with a photomultiplier (RCA C31034) which was combined with a photon counting system (16-bit resolution).[16] The IR absorption measurements at 6 K were carried out by a FT-IR spectrometer (Bruker IFS113). The synthesis of **1** was described in reference [17].

Received: August 24, 1998
Revised version: January 26, 1999 [Z12316IE]
German version: *Angew. Chem.* **1999**, *111*, 2758–2761

Keywords: carotenoids · fluorescence spectroscopy · laser spectroscopy · UV/Vis spectroscopy

[1] H. A. Frank, R. Farhoosh, R. Gebhard, J. Lutgenburg, D. Gosztola, M. R. Wasielewski, *Chem. Phys. Lett.* **1993**, *207*, 88.
[2] H. A. Frank, R. J. Cogdell in *Carotenoids in Photosynthesis* (Eds.: A. Young, G. Britton), Springer, London, **1992**.
[3] G. Marston, T. G. Truscott, R. P. Wayne, *J. Chem. Soc. Faraday Trans.* **1995**, *91*, 4059.
[4] R. Bensasson, E. J. Land, B. Maudinas, *Photochem. Photobiol.* **1976**, *23*, 189.
[5] P. Mathis, J. Kleo, *Photochem. Photobiol.* **1973**, *18*, 343.
[6] J. E. Lewis, Dissertation, Arizona State University, **1993**.
[7] R. McDiarmid, J. P. Doering, *J. Chem. Phys.* **1980**, *73*, 4192.
[8] H. Bettermann, *Spectrochim. Acta* **1994**, *50*, 1073.
[9] B. S. Hudson, B. E. Kohler, K. Schulten in *Excited States Vol. VI* (Ed.: E. Lim), Academic Press, New York, **1982**, p. 86.
[10] G. Herzberg, W. Teller, *Z. Phys. Chem. B* **1933**, *21*, 410.
[11] M. Bienioschek, Dissertation, Universität Düsseldorf, **1995**.
[12] W. Bouschen, Diplomarbeit, Universität Düsseldorf, **1996**.
[13] J. B. Birks, *Photophysics of Aromatic Molecules*, Wiley-Interscience, New York, **1970**.
[14] V. L. Ermolaev, *Sov. Phys. Usp. (Engl. Transl.)* **1963**, *80*, 333.
[15] S. Saito, M. Tasumi, *J. Raman Spectrosc.* **1983**, *14*, 310.
[16] H. Bettermann, I. Dasting, W. Rauch, *J. Chem. Phys.* **1993**, *99*, 1564.
[17] H. Bettermann, M. Bienioschek, H. Ippendorf, H.-D. Martin, *Angew. Chem.* **1992**, *104*, 1073; *Angew. Chem. Int. Ed. Engl.* **1992**, *31*, 1042.

